On the use of $^{14}CO\_2$ as a tracer for fossil fuel CO_2: Quantifying uncertainties using an atmospheric transport model

Jocelyn Turnbull, Peter Rayner, John Miller, Tobias Naegler, Philippe Ciais, Anne Cozic

On the use of $^{14}CO_2$ as a tracer for fossil fuel CO_2: Quantifying uncertainties using an atmospheric transport model

Jocelyn Turnbull,[1] Peter Rayner,[2] John Miller,[1,3] Tobias Naegler,[4] Philippe Ciais,[2] and Anne Cozic[2]

Received 23 April 2009; revised 24 July 2009; accepted 4 August 2009; published 17 November 2009.

[1] $\Delta^{14}CO_2$ observations are increasingly used to constrain recently added fossil fuel CO_2 in the atmosphere. We use the LMDZ global atmospheric transport model to examine the pseudo-Lagrangian framework commonly used to determine recently added fossil fuel CO_2 (CO_{2ff}). Our results confirm that $\Delta^{14}CO_2$ spatial variability in the Northern Hemisphere troposphere is dominated by the effect of CO_{2ff}, whereas in the Southern Hemisphere, ocean CO_2 exchange is more important. The model indicates that the free troposphere, at 3–5 km altitude, is a good choice for "background," relative to which the recently added fossil fuel CO_2 can be calculated, although spatial variability in free tropospheric $\Delta^{14}CO_2$ contributes additional uncertainty to the CO_{2ff} calculation. Comparison of model and observations suggests that care must be taken in using high-altitude mountain sites as a proxy for free tropospheric air, since these sites may be occasionally influenced by (polluted) boundary layer air, especially in summer. Other sources of CO_2 which have $\Delta^{14}C$ different than that of the atmosphere contribute a bias, which, over the Northern Hemisphere land, is mostly due to the terrestrial biosphere, whereas ocean CO_2 exchange and nuclear industry and natural cosmogenic production of ^{14}C contribute only weakly. The model indicates that neglecting this bias leads to a consistent underestimation of CO_{2ff}, typically between 0.2 and 0.5ppm of CO_2, with a maximum in summer. While our analysis focuses on fossil fuel CO_2, our conclusions, particularly the choice of background site, can also be applied to other trace gases emitted at the surface.

Citation: Turnbull, J., P. Rayner, J. Miller, T. Naegler, P. Ciais, and A. Cozic (2009), On the use of $^{14}CO_2$ as a tracer for fossil fuel CO_2: Quantifying uncertainties using an atmospheric transport model, *J. Geophys. Res.*, *114*, D22302, doi:10.1029/2009JD012308.

1. Introduction

[2] The radiocarbon content ($\Delta^{14}C$) of carbon dioxide (CO_2) provides a unique tracer for the carbon cycle. The ^{14}C is produced naturally in the upper atmosphere by interaction of atmospheric nitrogen with cosmic ray induced neutrons. After oxidizing to form ^{14}CO and then $^{14}CO_2$, it exchanges with other carbon reservoirs, and decays radioactively (with a half life of 5730 ± 40 years [*Godwin*, 1962]). *Suess* [1955] was the first to recognize that the addition of extremely old, ^{14}C-free, fossil fuel CO_2 (CO_{2ff}) to the atmosphere would strongly decrease $\Delta^{14}CO_2$. CO_2 fluxes from the ocean also have a negative effect on $\Delta^{14}CO_2$ in the natural atmosphere, as significant radioactive decay occurs during the residence time of a few hundred years [e.g., *Braziunas et al.*, 1995; *Stuiver et al.*, 1983]. However, the production of ^{14}C as a by-product of atmospheric nuclear weapons testing nearly doubled the ^{14}C content of the atmosphere in 1963 [*Levin et al.*, 1985], substantially perturbing the natural ^{14}C cycle as this "bomb ^{14}C" moved from the atmosphere into the oceans and biosphere [e.g., *Manning et al.*, 1990; *Levin et al.*, 1985; *Nydal and Lövseth*, 1983]. The rate of uptake of excess ^{14}C has been widely used to examine carbon exchange between the atmosphere and oceans [e.g., *Müller et al.*, 2008; *Sweeney et al.*, 2007; *Krakauer et al.*, 2006; *Naegler et al.*, 2006; *Hesshaimer et al.*, 1994; *Broecker et al.*, 1985] and biosphere [e.g., *Hahn and Buchmann*, 2004; *Gaudinski et al.*, 2000; *Trumbore*, 2000]. Today, however, the ^{14}C disequilibrium between atmosphere and surface reservoirs is small, and its effect on the atmospheric $\Delta^{14}CO_2$ trend and distribution is apparently smaller than that of fossil fuel CO_2 emissions [*Turnbull et al.*, 2007].

[3] A number of studies have taken advantage of this strong effect of fossil fuel CO_2 emissions on $\Delta^{14}C$ to constrain atmospheric mixing ratios of recently added CO_{2ff}, demonstrating that $\Delta^{14}C$ is likely to be the best method to independently and objectively verify fossil fuel CO_2 emissions [*Levin and Karstens*, 2007; *Levin et al.*, 2003; *Turnbull et al.*, 2006; *Hsueh et al.*, 2007; *Meijer et al.*,

[1]Earth Systems Research Laboratory, NOAA, Boulder, Colorado, USA.
[2]Laboratoire des Sciences du Climat et de l'Environnement, Gif-sur-Yvette, France.
[3]CIRES, University of Colorado at Boulder, Boulder, Colorado, USA.
[4]Institut für Umweltphysik, Heidelberg, Germany.

0148-0227/09/2009JD012308

1996; *Zondervan and Meijer*, 1996]. These measurements have an immediate application to verify compliance with fossil fuel CO_2 emissions targets such as the Kyoto Protocol [*Riley et al.*, 2008; *Levin and Rödenbeck*, 2007]. The improved constraint on CO_{2ff} mixing ratios is also useful for improving both bottom-up and top-down estimates of biospheric and ocean CO_2 exchange. The reported CO_{2ff} emissions have uncertainties of 5–20% at the national, annual scale [*Gregg et al.*, 2008; *Marland et al.*, 2006], and potentially much larger uncertainties at smaller spatial and temporal scales. Despite this, in a typical atmospheric CO_2 inversion framework, where atmospheric CO_2 mixing ratios are convolved with an atmospheric transport model to solve for the surface fluxes, the CO_{2ff} flux is usually assumed to be perfectly known [e.g., *Baker et al.*, 2006; *Gurney et al.*, 2002] so that any bias in the estimates of CO_{2ff} will contaminate estimates of the biospheric CO_2 flux. Atmospheric observations can potentially reduce this problem, either by relating observed atmospheric $\Delta^{14}CO_2$ values back to the CO_{2ff} emission flux, or by "correcting" observed total CO_2 mixing ratios for observed recently added CO_{2ff} (derived from $\Delta^{14}CO_2$). In this latter case, atmospheric observations directly constrain the recently added CO_{2ff} mixing ratio in each sample, minimizing the need for emissions inventories or knowledge of wind patterns, and this methodology can be applied equally to small-scale studies such as flux tower measurements of CO_2.

[4] To date, most researchers have used a straight forward approach to determining recently added CO_{2ff} from $\Delta^{14}CO_2$ observations, using a method based entirely on observations and independent of any explicit model [e.g., *Palstra et al.*, 2008; *Hsueh et al.*, 2007; *Turnbull et al.*, 2006; *Levin et al.*, 2003; *Meijer et al.*, 1996]. In this pseudo-Lagrangian method, a parcel of air with an initial CO_2 mixing ratio (CO_{2bg}) and $\Delta^{14}CO_2$ value (Δ_{bg}) moves across a polluted region, which modifies its CO_2 mixing ratio and $\Delta^{14}CO_2$ value to CO_{2obs} and Δ_{obs} by the addition of CO_{2ff} and any other sources or sinks of CO_2 (CO_{2other}), each with their own $\Delta^{14}C$ value (Δ_{ff} and Δ_{other}, the weighted mean $\Delta^{14}C$ of the other CO_2 sources), such that

$$CO_{2obs} = CO_{2bg} + CO_{2ff} + CO_{2other} \tag{1}$$

$$\Delta_{obs} CO_{2obs} = \Delta_{bg} CO_{2bg} + \Delta_{ff} CO_{2ff} + \Delta_{other} CO_{2other}. \tag{2}$$

Combining equations (1) and (2), Δ_{ff} is known to be -1000‰ (the $\Delta^{14}C$ value for zero ^{14}C content), and if CO_{2obs}, Δ_{obs} and Δ_{bg} are measured, CO_{2ff} can be calculated as

$$CO_{2ff} = \frac{CO_{2obs}(\Delta_{obs} - \Delta_{bg})}{\Delta_{ff} - \Delta_{bg}} - \frac{CO_{2other}(\Delta_{other} - \Delta_{bg})}{\Delta_{ff} - \Delta_{bg}}, \tag{3}$$

where the second term is the bias (β) due to the effect of CO_{2other}, such that

$$\beta = \frac{CO_{2other}(\Delta_{other} - \Delta_{bg})}{\Delta_{ff} - \Delta_{bg}}. \tag{4}$$

Here $\Delta^{14}C$ is defined according to *Stuiver and Polach* [1977] as

$$\Delta^{14}C = \left[\frac{\left({}^{14}C/C\right)_{samN}}{\left({}^{14}C/C\right)_{abs}} - 1 \right]. \tag{5}$$

$\Delta^{14}C$ is reported in per mil (‰) and $(^{14}C/C)_{abs}$ the ^{14}C:C ratio of the absolute radiocarbon dating standard (1.176×10^{-12} mol^{14}C/molC; and is related to the commonly used primary measurement standard Oxalic Acid I [*Karlen et al.*, 1968; *Stuiver and Polach*, 1977]). The $(^{14}C/C)_{samN}$ is the ^{14}C:C ratio in the sampled material, normalized to a $\delta^{13}C$ value of -25‰. This normalization mathematically corrects for the effects of isotopic fractionation, such that processes which naturally fractionate during exchange (e.g., photosynthetic uptake of CO_2) have no impact on atmospheric $\Delta^{14}C$, and thus only disequilibrium terms need to be considered.

[5] We note that the $\Delta^{14}C$ of photosynthetic uptake (gross primary productivity) is implicitly assumed to be equal to Δ_{bg}. This is strictly true in the limit that the time (and space) between background and observation goes to zero. Some authors [e.g., *Riley et al.*, 2008; *Kuc et al.*, 2007] have instead assumed that $\Delta^{14}C$ of photosynthesis is equal to Δ_{obs}, and in this case, equation (3) can be rewritten as

$$CO_{2ff} = \frac{CO_{2bg}(\Delta_{obs} - \Delta_{bg})}{\Delta_{ff} - \Delta_{obs}} - \frac{CO_{2other}(\Delta_{other} - \Delta_{obs})}{\Delta_{ff} - \Delta_{obs}}. \tag{6}$$

When integrated $\Delta^{14}CO_2$ sampling is used, this formulation may be advantageous, as CO_{2obs} is not required. In the case of flask sampling, CO_{2obs} will usually be measured, so equation (3) is more convenient. If CO_{2other} is zero, then equations (3) and (6) are exactly equivalent, but slight differences of up to 0.1 ppm in CO_{2ff} can occur when both photosynthetic uptake of CO_2 and the ($\Delta_{obs} - \Delta_{bg}$) difference are large. As this difference is much smaller than the other uncertainties discussed here, we will not discuss it further.

[6] Uncertainties in the CO_{2ff} calculation method come primarily from statistical $\Delta^{14}C$ measurement uncertainties, which are currently at best about 2‰ [*Graven et al.*, 2007; *Turnbull et al.*, 2007; *Levin and Kromer*, 1997], which translates to an uncertainty in CO_{2ff} of 0.7 ppm for a single measurement. Additional uncertainty and potentially large biases come from the estimate of β and from the choice of Δ_{bg}. Note also, that when equation (6) is used, the choice of CO_{2bg} will also play a role, and we will treat this in a future paper.

[7] For land regions, where most fossil fuel emissions occur, heterotrophic respiration, with it's potentially large ^{14}C disequilibrium, is expected to be the main contributor to β. Some authors have assumed that $\beta = 0$ (i.e., all other sources have $\Delta^{14}C$ equal to that of the background atmosphere and $\Delta_{other} = \Delta_{bg}$) [e.g., *Levin et al.*, 2003], but others have estimated β values for heterotrophic respiration, such that if β is ignored, CO_{2ff} would be consistently underestimated by up to 0.5 ppm in summer and 0.2 ppm in winter [*Palstra et al.*, 2008; *Riley et al.*, 2008; *Hsueh et al.*, 2007; *Turnbull et al.*, 2006].

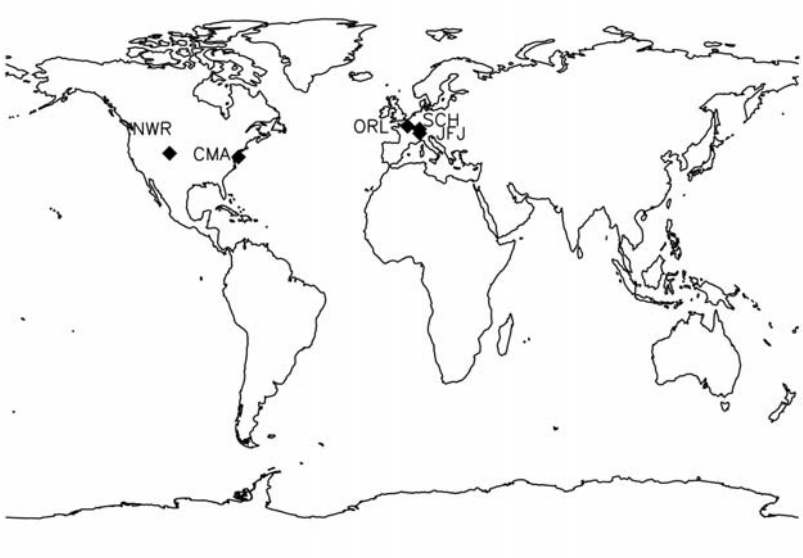

Figure 1. Locations of sampling sites discussed in this paper: NWR, Niwot Ridge, Colorado; CMA, Cape May, New Jersey; ORL, Orleans, France; SCH, Schauinsland, Germany; JFJ, Jungfraujoch, Switzerland.

[8] The pseudo-Lagrangian framework assumes that the upwind Δ_{bg} value can be measured, yet this is not possible or practical in most situations. For example, in the case of integrated samples collected over days to months (e.g., from plant material or integrated air sampling) the upwind region will likely have varied through the sampling period. Even for flask samples, the air parcel received at the observing site is a mixture of air received from a footprint region, rather than from a single point location. Thus we usually select samples collected at approximately the same time at a "clean air" background location to represent Δ_{bg}. The dearth of such measurements, and of continental surface locations sufficiently far from pollution sources, means that the high-altitude sites at Jungfraujoch, Switzerland (JFJ), and Niwot Ridge, Colorado, United States (NWR), have been most commonly used as European and North American background $\Delta^{14}CO_2$ sites, respectively. Both sites are at ~3500 m altitude. Schauinsland, Germany (SCH, 1205 masl [*Levin and Kromer*, 1997]) measurements have also been used for Δ_{bg} when other data has not been available [*Kuc et al.*, 2007], although 2–3 ppm of CO_{2ff} is regularly detectable in samples from this site relative to JFJ [*Levin and Rödenbeck*, 2007], thus biasing CO_{2ff} estimates by the same amount. Figure 1 shows the location of these two sites, and others discussed in this paper.

[9] While the biases and uncertainties in the pseudo-Lagrangian calculation of CO_{2ff} have been identified, they have not been quantitatively evaluated. Here we use the global atmospheric transport model LMDZ to simulate $\Delta^{14}CO_2$ and these biases and uncertainties. In section 2, we describe the model and methods used to model $\Delta^{14}CO_2$. We then demonstrate, in section 3.1, that our model reasonably simulates atmospheric $\Delta^{14}CO_2$, and in section 3.2, that the surface spatial distribution of $\Delta^{14}CO_2$ in the Northern Hemisphere is strongly dominated by the effect of fossil fuel CO_2 emissions. In section 3.3, we examine how the choice of background site can influence the calculation of CO_{2ff}, focusing on the choice of free tropospheric and high mountain sites as background. While we focus specifically on CO_{2ff}, these results may also apply to other trace gas species which are emitted at the surface. In section 3.4, we examine the impact of systematic errors from other CO_2 sources, notably the terrestrial biosphere, as represented by the second, bias term (β) in equation (1).

2. Methods

[10] We use the LMDZ4/INCA.2 global atmospheric transport model, described in detail by *Hourdin et al.* [2006] and *Hauglustaine et al.* [2004]. The model resolution is 2.5° × 3.75°, with 19 vertical layers, including four layers in the first kilometer above the surface, a mean vertical resolution of about 2 km between 2 and 20 km, and four layers above 20 km. The model calculates its own meteorology, and the horizontal wind fields are then "nudged" every 6 h by the ECMWF reanalysis winds. The previous moist convection scheme has been replaced by a new implementation of *Emanuel*'s [1991, 1993] moist convective mixing parameterization. Although LMDZ and INCA are coupled, chemistry is turned off in these simulations. The model has been validated for CO_2 transport, and compared with the TransCom intercomparison results [*Bousquet et al.*, 2008; *Gurney et al.*, 2002]. LMDZ4/INCA.2 is on the low end of the TransCom model range for interhemispheric CO_2 gradient and does not always capture a large enough vertical gradient in CO_2 over the continents, apparently due to an overestimate in the modeled height of the planetary boundary layer. This type of problem is common to all the TransCom models, none of which obtain accurate CO_2 vertical gradients at all locations in all seasons [*Stephens et al.*, 2007]. This is the major weakness of the model for our application, and will result in smaller modeled surface horizontal gradients than expected, as well as an underestimate of vertical differences, particularly in the biases discussed in section 3.4. LMDZ4/INCA.2 does agree quite well with observations in the free

Table 1. Effect of Each Source on the Mean Global Atmosphere $\Delta^{14}CO_2$[a]

	Model Run		
	Standard	Lowbio	Highbio
Fossil fuels	−10.5	−10.5	−10.5
Terrestrial biosphere	2.6	2.0	4.0
Oceans	−2.6	−2.0	−4.0
Cosmogenic production	5.2	5.2	5.2
Nuclear industry	0.5	0.5	0.5
Total	−4.8	−4.8	−4.8

[a]In per mil per year. Calculated effect on mean global $\Delta^{14}CO_2$ is based on an atmosphere with an initial $\Delta^{14}CO_2$ value of 60‰ and 375 ppm of CO_2. In the lowbio and highbio scenarios the ocean ^{14}C flux is tuned to conserve the global trend.

troposphere. As with most large-scale models, LMDZ4/INCA.2 has difficulty simulating nighttime boundary layer CO_2 values. Agreement between model and surface observations is better in summer than in winter, again likely related to the modeled boundary layer height. As with all global models of low resolution, it fails to adequately capture variability at some continental sites close to variables sources [*Geels et al.*, 2007]. Despite these limitations, the model captures large-scale CO_2 variability quite well, and falls within the range of TransCom models. This model version appears to be a significant improvement over the previous off-line version LMDZ3 [*Bousquet et al.*, 2008]. Despite the known problems with modeled vertical transport, the CO_2 mixing ratios at our sites are captured quite well in the model, and discussed in further detail in section 3.1.

[11] We transport fluxes of CO_2 and $^{14}CO_2$ separately in the model, and $\Delta^{14}C$ is calculated from these offline, following equation (5). In the model, we implicitly include the normalization correction in the $^{14}CO_2$ fluxes, except in the case of the fossil fuel CO_2 flux, where we specify no isotopic information, since it contains no ^{14}C. This means that we do not account for the ^{13}C Suess effect, of 0.025‰ yr^{-1} (ftp://ftp.cmdl.noaa.gov/ccg/co2c13/GLOBALVIEW/), which would change $\Delta^{14}CO_2$ by less than 0.04‰ yr^{-1}. We do account for the change in $^{14}CO_2$ mixing ratio due simply to the change in CO_2 mixing ratio over time (e.g., biospheric uptake of CO_2 removes CO_2 seasonally, decreasing the $^{14}CO_2$ mixing ratio, although it does not change $\Delta^{14}CO_2$), calculating the effect of this at each model time step. The impact on $\Delta^{14}C$ of each individual ^{14}C source is estimated by calculating the $\Delta^{14}CO_2$ value in the case where all other sources have $\Delta^{14}C$ values the same as the atmosphere.

[12] We use CO_2 and $^{14}CO_2$ fluxes based on those described by *Turnbull et al.* [2009] with some alterations, and also include a $^{14}CO_2$ flux from the nuclear industry.

[13] The net oceanic CO_2 flux is derived from ΔpCO_2 [*Takahashi et al.*, 2002]. The net flux from the terrestrial biosphere is taken from the CASA biogeochemical model, set to result in a neutral biosphere [*Gurney et al.*, 2002]. The annual global total fossil fuel CO_2 emissions are from *Marland et al.* [2006] until 2003 and then linearly extrapolated to 2007. This flux is spatially distributed according to the EDGAR inventories from 1995 and 2000 (http://www.rivm.nl/edgar/) [*Olivier and Berdowski*, 2001], and have a ∼20% seasonal cycle with it's maximum in the Northern Hemisphere winter. This seasonal cycle is based on that reported by *Blasing et al.* [2005] for the United States, and is in reasonable agreement with inventory data for Europe [*Peylin et al.*, 2009].

[14] The $^{14}CO_2$ fluxes are from natural cosmogenic production, the nuclear industry (power generation and reprocessing plants), ^{14}C ocean disequilibrium and heterotrophic respiration from the biosphere. We neglect the -0.1‰ yr^{-1} effect of radioactive decay of ^{14}C in the atmosphere. Each $^{14}CO_2$ global annual flux is rescaled to approximately match those calculated using the GRACE box model [*Naegler and Levin*, 2006] for our period of simulation 2002–2007. An initial uniform global background $\Delta^{14}CO_2$ value was assigned in the model, and set such that the modeled absolute $\Delta^{14}CO_2$ trend is in agreement with the observations at JFJ (see section 3.1). All fluxes are regridded to match LMDZ. The effect of each modeled ^{14}C flux, as well as that of the ^{14}C-free fossil fuel CO_2 flux, on the mean global $\Delta^{14}CO_2$ is shown in Table 1.

[15] The $^{14}CO_2$ terrestrial heterotrophic respiration term is first estimated using pulse-response functions from the CASA biosphere model for the year 2004 [*Thompson and Randerson*, 1999] and the time history of atmospheric $\Delta^{14}CO_2$ [*Levin and Kromer*, 2004]. We then scale the resulting spatial and seasonal distribution to match the best estimate of the total $^{14}CO_2$ flux predicted by the GRACE model for this time period [*Naegler and Levin*, 2006, 2009]. This is our standard ("standard") case, with total annual impact of the biosphere on the atmosphere of 2.6‰ yr^{-1}. In addition, we test the sensitivity of our results to uncertainty in this flux, using the lowest ("lowbio") and highest ("highbio") reasonable values as determined by the GRACE box model and atmospheric observations. We note that although fire CO_2 emissions may have a much larger $\Delta^{14}CO_2$ disequilibrium than heterotrophic respiration, due to the longer residence time of carbon in forests, fire CO_2 flux is quite small. We calculate that the effect on global atmospheric $\Delta^{14}CO_2$ of the 0.2 GtC yr^{-1} global fire CO_2 flux [*Balshi et al.*, 2007] with a fire return frequency of 200 years in boreal forests (i.e., $\Delta^{14}C$ of −24‰) is about 0.02‰ yr^{-1}. Hence, we fold this flux into the heterotrophic respiration flux.

[16] The gross ocean-to-atmosphere $^{14}CO_2$ flux was first estimated using climatological surface ocean pCO_2 [*Takahashi et al.*, 2002], an assembly of surface ocean $\Delta^{14}C$ of dissolved inorganic carbon (DIC) measurements from the GLODAP project (cdiac.ornl.gov/oceans/glodap/Glodap_home.htm), and the gas transfer formulation of *Wanninkhof* [1992]. Since the GLODAP data set is based on measurements from the 1970s and 1990s, we expect that the $^{14}CO_2$ flux into the ocean is now much lower than this estimate. To account for this, we scale the spatial and seasonal distribution downward to match our annual total flux estimates (Table 1). Since this flux has very little impact on the Northern Hemisphere spatial distribution of $\Delta^{14}CO_2$, in our lowbio and highbio cases, we scale the ocean flux to maintain the observed trend in $\Delta^{14}CO_2$, but retaining the seasonal and spatial patterns.

[17] Cosmogenic production of 350 mol ^{14}C/yr occurs throughout the atmosphere, with maximum production at the magnetic poles and a minimum at the equator. We distribute the $^{14}CO_2$ production horizontally following *Masarik and Beer* [1999], with the production rate (per mole of air) increasing linearly from zero at five kilometers

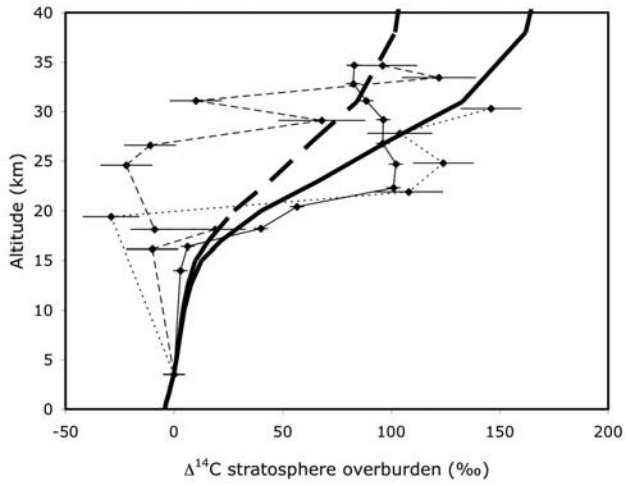

Figure 2. Deviations of $\Delta^{14}CO_2$ from the surface value. The modeled vertical distribution over Sanriku, Japan, for 2006 is shown as the thick solid line. The thick dashed line shows the modeled vertical distribution when the cosmogenic production flux is forced to lower altitudes. Three observed $\Delta^{14}CO_2$ stratospheric profiles are shown as diamonds and error bars, connected by thin lines: 1989 (dotted line), 1990 (dashed line), and 1994 (solid line), and each is compiled from stratospheric observations collected over Sanriku, Japan [*Nakamura et al.*, 1992, 1994; *Turnbull*, 2006], and an associated monthly mean value from Jungfraujoch, Switzerland [*Levin and Kromer*, 2004]. Diamonds and error bars indicate the observed values and their measurement uncertainties. Each profile is presented as the deviation from the observed $\Delta^{14}C$ value at JFJ at the same time or the modeled value at 3.5 km.

to a maximum at the top of the model stratosphere. Figure 2 shows that our modeled vertical profile of $\Delta^{14}C$ agrees fairly well with the very few stratospheric $\Delta^{14}CO_2$ observations made in recent years [*Nakamura et al.*, 1994, 1992]. Although this vertical distribution weights the $^{14}CO_2$ production to somewhat higher altitudes than theory suggests [*Masarik and Beer*, 1999; *Lal*, 1988], when we applied a vertical distribution with more production close to the surface, our model did not build up enough ^{14}C in the stratosphere (Figure 2). We further discuss the impact of the vertical distribution of this flux on our results in section 3.3.

[18] An estimation of the small ^{14}C production flux from the nuclear industry is also included in the model. Both $^{14}CH_4$ and $^{14}CO_2$ are emitted by the nuclear power industry, with estimates of the total global production ranging from 45 to 85 mol ^{14}C/yr in 2000 [*UNSCEAR*, 2000]. Differing from the GRACE box model result, we use a low estimate of the total annual, global production of 45 mol ^{14}C yr^{-1}, and distribute it evenly across the 30°N–60°N landmasses. Our total flux is likely too low, especially since nuclear power generation is increasing by about 3% per year, but we use this low value to account, in a simplistic way, for two things. First, many operable nuclear reactors are pressurized water reactors [*International Atomic Energy Agency* (*IAEA*), 2004], which emit $^{14}CH_4$, rather than $^{14}CO_2$ [*UNSCEAR*, 2000]. The long atmospheric lifetime of CH_4 means that these emissions, while contributing to the overall trend in $^{14}CO_2$, are unlikely to contribute a strong signal in $^{14}CO_2$ at the surface. Since we do not model $^{14}CH_4$ oxidation, our low flux estimate is designed to account for this issue. Second, while it is known that the emission rate of ^{14}C varies with the type of reactor [*UNSCEAR*, 2000], it is not clear how much variability there might be between reactors of a single type, and whether the emissions are constant through time, or occur as discrete, large pulses of ^{14}C. In the absence of better data, we do not attempt to distribute the emissions by point source, instead, we use a lower total emissions estimate, distributed evenly across the midlatitudes, noting that close to nuclear ^{14}C sources, substantially larger emissions will occur, which are not accounted for in our model.

[19] The model is initiated with evenly distributed $\Delta^{14}CO_2$, with the initial value set to obtain the best match with the annual mean JFJ values. The choice of site for tuning of the initial value is somewhat arbitrary, but comparison with the other sites (section 3) demonstrates that it is a reasonable choice. After a 2 year "spin-up" to remove the effect of the initial condition of $\Delta^{14}CO_2$, we obtained model results for 2002–2007, and we extract the monthly mean values. We do not consider a longer time series, because we are specifically interested in examining the recent time period when fossil fuel emissions dominate the $\Delta^{14}CO_2$ variability. During this time period, when the biosphere and ocean ^{14}C disequilibriums with the atmosphere are reasonably small (because the bomb ^{14}C is now quite well distributed throughout the reservoirs), we can consider them to be constant.

[20] When comparing our modeled results with mountaintop sampling sites, the mismatch between the modeled and real-world surface topography needs to be taken into account [*Law et al.*, 2008; *Geels et al.*, 2007]. While NWR and JFJ are both situated at 3500 masl, the modeled surface altitude of the grid box is 1600 m for NWR, and 500 m JFJ. To select the most appropriate model level at each site, we use the method described by *Taylor* [2001], whereby observations of both the CO_2 mixing ratio seasonal cycle phase and its amplitude are compared with those at each model level, following

$$E = \sigma_{obs}^2 + \sigma_{mdl}^2 - 2\sigma_{obs}\sigma_{mdl}R. \quad (7)$$

E is the root mean square error; σ_{obs} and σ_{mdl} are the standard deviations of the detrended seasonal cycle for the observations and model level. R is the correlation coefficient of the fit between the observed and model level values. The standard deviations capture the difference in the seasonal amplitude, and R captures the difference in the seasonal cycle phase. The best model level is determined as that where E is minimized; that is, the differences in phase and amplitude between observations and model are smallest. We select model level 2 (450 m above model ground) SCH, and model level 4 (1500 m above model ground) for JFJ (Figure 3). At NWR, E has the same minimum value for levels 2 and 3; we select level 2, as the phase agreement is slightly better, but this indicates that the choice of model level is not critical. In all cases, the selected model level is above the model surface, but below the true sampling site altitude, consistent with expectations. The

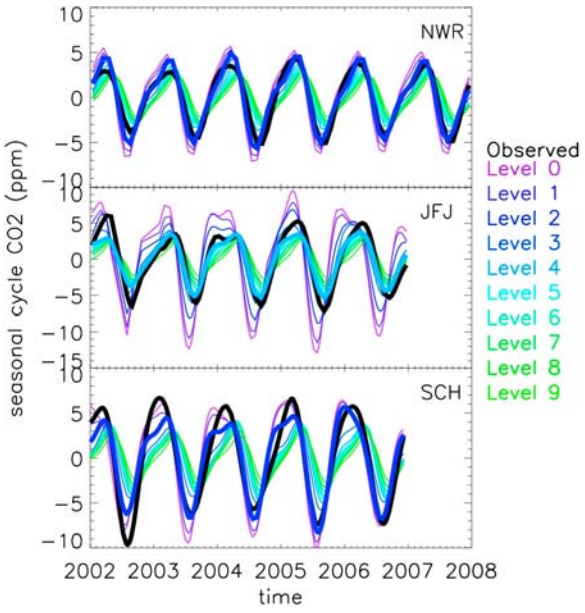

Figure 3. CO_2 seasonal cycles for the three high-altitude sites discussed here. We select the most appropriate model level for the site as the level where the phase and amplitude of the CO_2 seasonal cycle best agree with observations [*Taylor*, 2001]. Each level is shown as a thin colored line, and the thick colored line is the chosen level.

agreement between the selected model level and the observed CO_2 seasonal cycle phase is good for all sites. There is a slight underestimate in the seasonal amplitude at JFJ and SCH, likely because the model biosphere flux values we used have slightly too small a magnitude, whereas the phase in this flux may be more reliable [*Gurney et al.*, 2004]. Again, we note that LMDZ, along with other global transport models, has some difficulty in obtaining the correct magnitude of vertical gradients over the continental land. Because we are selecting for the model level that best matches the observations, our method actually reduces the impact of this problem. We also tested for the impact of choosing an adjacent model level where the fit is slightly poorer but still reasonable, and for averaging two adjacent model levels; this did not significantly impact our interpretations.

3. Results and Discussion

3.1. Comparison of Modeled and Observed $\Delta^{14}CO_2$

[21] The modeled $\Delta^{14}CO_2$ values at three sites where observations are available for most of our modeled time period (Niwot Ridge, Colorado, United States, Jungfraujoch, Switzerland, and Schauinsland, Germany) are compared with the observations in Figure 4. As described in section 2, the model was tuned such that the modeled absolute $\Delta^{14}CO_2$ trend is in agreement with the observations at JFJ. This results in good agreement between model and observations at the other sites. The larger scatter in observations at NWR may be due to the difference in sampling method: at JFJ and SCH, the observations are integrated monthly mean values [*Levin et al.*, 2008], whereas at NWR, measurements were taken from weekly flask samples [*Turnbull et al.*, 2007]. The overall downward trend agrees well with the observations at all sites, decreasing by 5‰/yr, an unsurprising result since we tuned the flux fields to obtain the observed trend. The difference between the sites is well captured, and the seasonal cycle also appears reasonable. At these mountain sites, the impact of possible biases in modeled vertical transport (described in section 2) is small, because they lie mostly in the free troposphere. This suggests that our model fluxes are realistic, and allows us to use the model to further examine $\Delta^{14}CO_2$ as a proxy for fossil fuel CO_2 concentration deviation from background (see equation (3)).

3.2. Spatial Distribution of $\Delta^{14}CO_2$

[22] The mean LMDZ modeled surface $\Delta^{14}CO_2$ values for 2002–2007 are shown in Figure 5. Figure 5 shows the lowest model level, representing the surface; this is comparable in both pattern and magnitude of the spatial distribution to the next model level up (~180 m above model surface). In the Southern Hemisphere, the spatial variability is quite weak, but dominated by the effect of ocean disequilibrium. In the Northern Hemisphere, $\Delta^{14}CO_2$ variability is strongly dominated by the effect of (^{14}C-free) fossil fuel emissions, with the lowest values in regions where fossil fuel emissions occur, and gradual increases in the $\Delta^{14}CO_2$ values downwind from the source regions. This strong relationship can be clearly seen by comparison with

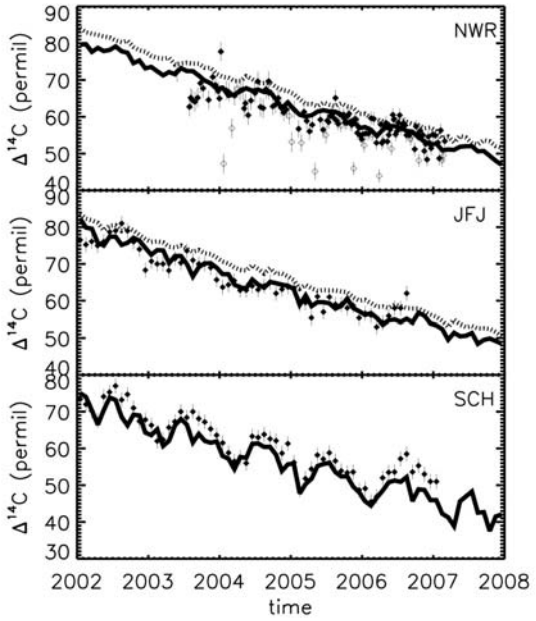

Figure 4. Comparison of modeled and observed $\Delta^{14}CO_2$ time series for three Northern Hemisphere sites. Solid lines are the modeled monthly mean $\Delta^{14}CO_2$ values for each site. Symbols are the observed $\Delta^{14}CO_2$ values for each site and are reproduced from *Turnbull et al.* [2007] for NWR, and from *Levin et al.* [2008] for JFJ and SCH. Open symbols at NWR indicate samples that were identified as containing local pollution. Error bars are the reported 1-sigma error on the ^{14}C measurement. Dotted lines are the modeled value for 3.5 km altitude free tropospheric air over the eastern United States at NWR and over Western Europe at JFJ.

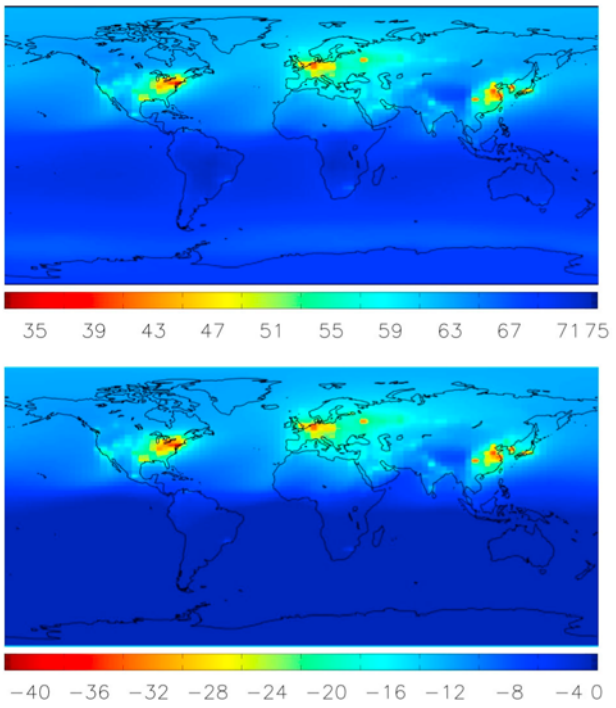

Figure 5. (top) Modeled mean surface distribution of $\Delta^{14}CO_2$ for 2002–2007. (bottom) Modeled surface distribution of $\Delta^{14}CO_2$ if fossil fuel CO_2 emissions were the only source of variability in $\Delta^{14}CO_2$; values are shown relative to the equator. Note that the scale range is identical (40‰) in both plots, and the surface level is taken as the lowest model level.

Figure 5 (bottom), which shows the spatial variability in $\Delta^{14}CO_2$ due only to fossil fuel emissions (i.e., when all other CO_2 sources have $\Delta^{14}C$ values equal to that of the atmosphere). Not only the spatial pattern, but also the magnitude of the $\Delta^{14}CO_2$ differences in the Northern Hemisphere, are comparable between the two modeled distributions shown in Figure 5. As discussed earlier, the choice of model level can have substantial impact on the $\Delta^{14}CO_2$ values for mountain sites, where the model resolution is unable to capture the topography correctly. For the global distribution, this impacts only a few discrete locations.

[23] The spatial distribution is in general agreement with $\Delta^{14}CO_2$ observations over Northern Hemisphere land, capturing the broad continental variability in the observations (Figure 6). The large-scale model is unable to adequately resolve fine structure, such as the very low $\Delta^{14}C$ values observed close to large cities (e.g., in California, and also in comparison to fine-scale $\Delta^{14}CO_2$ distributions obtained from wine ethanol in Europe [*Palstra et al.*, 2008]). The model does not always capture the magnitude of the spatial variability particularly well, and this is likely related to the known biases in the modeled vertical transport [*Turnbull et al.*, 2009]. However, our results are similar to other model predictions for the 1990s and 2000s [*Hsueh et al.*, 2007; *Randerson et al.*, 2002].

3.3. Choice of Background Site

[24] CO_{2ff} in equation (3) is the fossil fuel CO_2 added relative to a background site, and the choice of background site thus strongly influences the calculated CO_{2ff}. In today's atmosphere (with ~380 ppm of CO_2 and Δ_{bg} of ~60‰), a +1‰ bias in Δ_{bg} will result in an overestimate in CO_{2ff} of +0.3 ppm. This is the same change in CO_{2ff} as caused by an equal, opposite change in Δ_{obs} of −1‰.

[25] Since it is difficult to identify surface sites which are not influenced by local sources, most researchers have assumed that free tropospheric observations, and high mountain sites as a proxy for the free troposphere, represent a reasonable background relative to which the recently added fossil fuel CO_2 in boundary layer air can be determined. We use the model to test how well these locations represent "background."

[26] First, we consider the best choice of altitude for free troposphere "background" sites. Cosmogenic production of $^{14}CO_2$ results in a vertical change in $\Delta^{14}CO_2$, with increasing values in the upper atmosphere, especially in the stratosphere (Figure 2), and a background site too high in the troposphere might be influenced by this effect. Figure 7 shows the modeled Northern Hemisphere mean vertical distribution of $\Delta^{14}CO_2$ from the surface to 10 km altitude, if CO_{2ff} emissions are excluded from the model. The vertical change is less than 1‰, with negative values (relative to the surface) in the lower troposphere, due to the influence of surface fluxes of biospheric respiration and nuclear industry $^{14}CO_2$. Above about 7 km, however, the $\Delta^{14}CO_2$ values begin to increase, due to the cosmogenic ^{14}C flux, which strongly dominates in the stratosphere (see Figure 2). This does not change substantially if the cosmo-

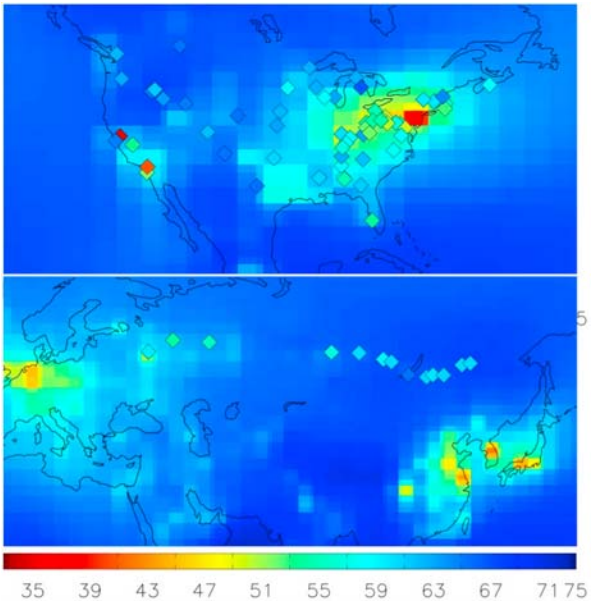

Figure 6. Comparison of observed $\Delta^{14}CO_2$ spatial distribution with the model. Observed values are the colored diamonds, superimposed on the modeled distribution. (top) Mean modeled values for North America during May–June–July 2004, compared to $\Delta^{14}CO_2$ values inferred from Zea mays collected in July/August 2004 [*Hsueh et al.*, 2007]. (bottom) Mean modeled values for Eurasia during March–April 2004, compared to $\Delta^{14}CO_2$ values from air samples collected from the trans-Siberian railway during March–April 2004 [*Turnbull et al.*, 2009].

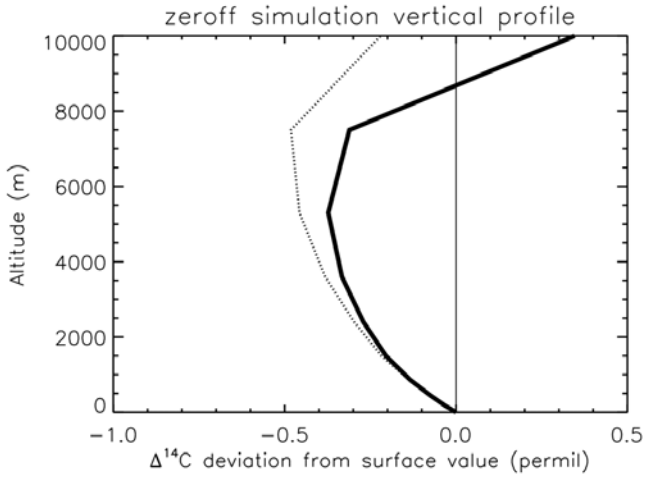

Figure 7. Northern Hemisphere mean vertical profile of $\Delta^{14}CO_2$ if no CO_{2ff} emissions occurred (thick black line, "zeroff simulation"), from the surface to 10 km. Dotted line is the same, except that the cosmogenic production field is altered to have more production in the lower atmosphere. Both profiles are normalized to their surface value.

genic production is weighted closer to the surface (Figure 7). Therefore, we recommend that altitudes below 6 km be used for the background site, to avoid any possibility of bias from cosmogenic production. To also avoid influence from the planetary boundary layer, free tropospheric sites above about 3 km should be used. We select ~3.5 km altitude because most aircraft sampling programs are able to routinely collect samples at this altitude, and this is the approximate altitude of several existing high mountain sampling sites.

[27] The Northern Hemisphere free troposphere is relatively well mixed with respect to $\Delta^{14}CO_2$ (Figure 8), with variability across the midlatitudes of about 3‰ (noting the exception over Central Asia where the high mean surface altitude influences the 3.5 km level), an order of magnitude smaller than the surface spatial variability of 38‰. Although this variability will be difficult to distinguish with current measurement uncertainties, it immediately indicates that care should be taken in the choice of background site, since it may bias CO_{2ff}.

[28] To more closely examine the choice of free tropospheric background over Northern Hemisphere land, we use model results from two example sites. These are selected to represent "typical" sampling locations, where both biological CO_2 emissions and fossil fuel CO_2 emissions occur nearby, and regular aircraft sampling of boundary layer and free tropospheric air already occurs (only model data is shown here). Our sites are: Cape May, New Jersey, UNITED STATES (CMA, 38.83°N, 74.31°W), on the North American eastern seaboard; and Orleans, France (ORL, 48.83°N, 2.5°E), just south of Paris (Figure 1). Figure 9 (middle) shows the modeled $\Delta^{14}CO_2$ differences between the surface site of interest and the free troposphere at 3.5 km above the site due to all sources other than CO_{2ff}. Small wintertime biases from cosmogenic production and nuclear industry sources, roughly cancel one another out, and are apparently due to the strong continental boundary layer buildup in winter. As noted earlier, the nuclear industry ^{14}C flux is uncertain and poorly represented in the model. Since the source is either very local ($^{14}CO_2$ emissions from the power plant point sources) or very dispersed throughout the atmosphere (oxidation of $^{14}CH_4$ emissions), in fact, its effect may be smaller at most sites, even if we underestimated the total emissions. The dominant effect is from the biosphere, for which the source is roughly colocated with the fossil fuel emissions we are interested in. The effect is strongest in summer, when respiration is high, and much weaker in winter. When any free troposphere site is used as background, this biospheric contribution cannot be avoided, and instead, we use a model to estimate and correct for it in the second term in equation (3). This is discussed in detail in section 3.4.

[29] High-altitude mountain sites have been assumed to represent free tropospheric air, and are most commonly used to determine Δ_{bg} [e.g., *Palstra et al.*, 2008; *Hsueh et al.*, 2007; *Kuc et al.*, 2007; *Levin et al.*, 2008]. Mountain sites do not, however, provide a perfect proxy for the free troposphere background, since they may be influenced more quickly by vertical mixing from the local surface than is the case for the same altitude in the free troposphere over a low-altitude surface. Using the LMDZ simulation, we test how well the NWR and JFJ sites represent free tropospheric air over our "typical" sites in North America and Europe. Comparison of the modeled NWR $\Delta^{14}CO_2$ with the 3.5 km level over the eastern United States shows that NWR is typically 1–2‰ lower than the eastern U.S. free troposphere, and in winter, and exhibits a much stronger seasonal cycle (Figure 4). A similar pattern is seen when JFJ is compared with the western European free troposphere. In both cases, the modeled difference is almost entirely due to fossil fuel CO_2 emissions, indicating that both of these mountain sites are slightly influenced by local fossil fuel emissions. The simulated bias depends on the model level chosen to represent these sites, and the magnitude of the biases would differ by ~1‰ if a different model level was selected (see section 2). Nevertheless, the model result indicates that mountain sites are not a perfect proxy for free tropospheric air.

[30] The observational records from NWR and JFJ suggest that there may also be substantial local surface influence during summer which is not seen by our large-scale model, likely due to sub-grid-scale vertical mixing events not captured at our model resolution. This is clear in the comparison of the model with the observed NWR values.

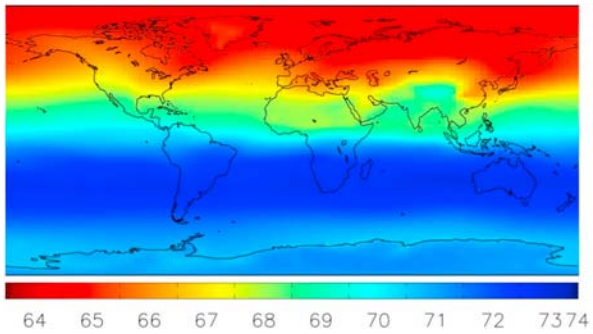

Figure 8. Modeled $\Delta^{14}CO_2$ distribution at 3.5 km altitude level. Note the scale change relative to Figures 5 and 6.

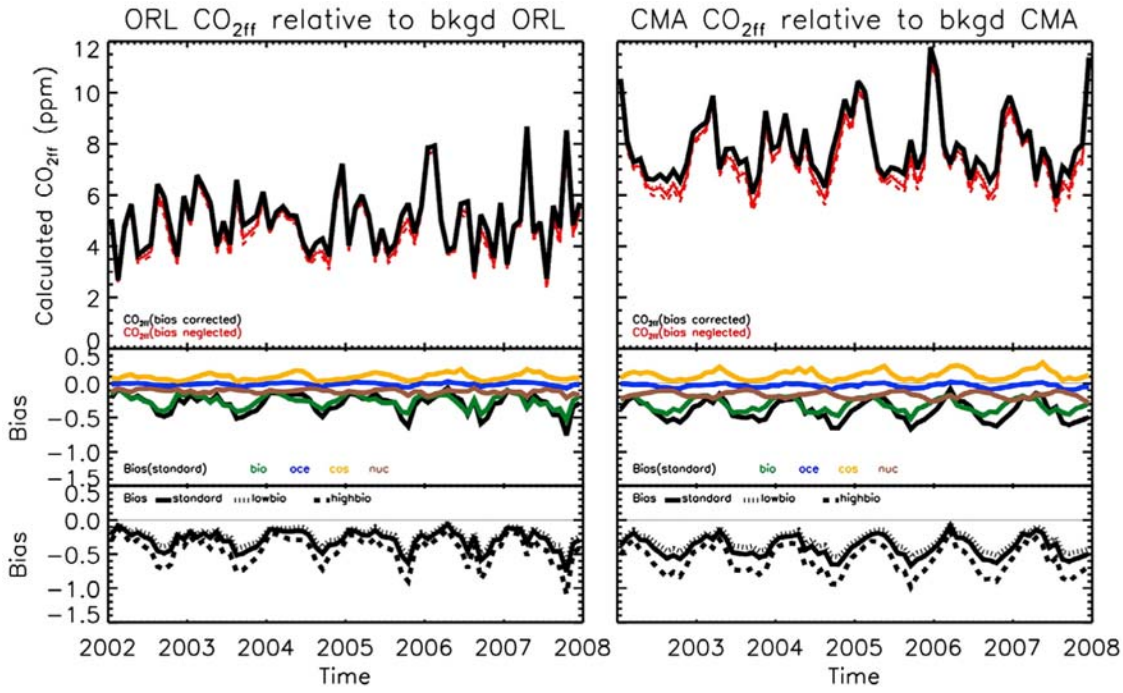

Figure 9. Calculated CO_{2ff} values at CMA and ORL. (top) The calculated CO_{2ff} at the surface level, using the 3.5 km level as background. Black lines are CO_{2ff} calculated when the bias term β is included in the calculation, and the red lines are the calculated CO_{2ff} when β is neglected, for the standard (solid line), highbio (dashed line), and lowbio (dotted line) scenarios. (middle) The bias in ppm of CO_2 (black line) and the contributions of each ^{14}C flux to the total bias. (bottom) The bias due to the biosphere ^{14}C flux, for the three scenarios.

The model agrees quite well with the "cleaned" data set (solid symbols in Figure 4), but does not reproduce the low values associated with local pollution events (open symbols in Figure 4) when air from the nearby Denver metropolitan region is lofted to the NWR site, and identified by elevated carbon monoxide mixing ratios [*Turnbull et al.*, 2007]. Including these locally polluted samples in the calculated monthly mean depresses the springtime monthly mean NWR values by 2 to 4 ‰, changing interannually depending on the frequency and strength of these local pollution events. The much longer JFJ record (started in 1986 [*Levin et al.*, 2008]) shows similar fluctuations in the magnitude of the spring decrease in $\Delta^{14}CO_2$. Since these samples are collected as integrated biweekly or monthly means, it is not possible to positively identify local pollution events in the $\Delta^{14}CO_2$ record, but local pollution events bringing air from the (populated) valley below can be seen in other proxies [*Lugauer et al.*, 2000, 1998]. This supports the possibility that interannual variability in the strength of springtime drawdown in $\Delta^{14}CO_2$ at JFJ may be related to the frequency and strength of such local pollution events.

[31] We also note that incursions of stratospheric air, which is enriched in ^{14}C, could cause similar, but opposite biases from time to time at these high-altitude sites. For example, during synoptic dry intrusions, stratospheric air can be delivered even to surface sites, but is not likely to be well captured by large-scale models [*Stohl*, 2001].

[32] It is apparent that when remote and/or high-altitude sites are used to represent the background, care should be taken to ensure that seasonal transport effects such as those described above are identified and/or avoided. We suggest that conditional integrated sampling, which samples the air only during periods identified as from a clean air sector, or alternatively, flask sampling, where individual polluted samples can be positively identified, provide the best likelihood of obtaining the most representative "background" air.

[33] The modeled differences of 1–3‰ due to the choice of background site are similar to or smaller than current measurement uncertainties, but they will result in biases, rather than random variability. Since equation (3) calculates recently added fossil fuel CO_2, as the CO_{2ff} overburden relative to the background used, the choice of background site is critical to the interpretation of the results. This does not preclude the use of remote or mountain sites as background, and indeed these sites will likely continue to provide the best available estimates of background $\Delta^{14}CO_2$ values for the Northern Hemisphere.

[34] We do suggest, however, that in light of the differences between background sites, and particularly the apparent seasonality of the differences between sites, care should be taken in selection of the appropriate background site for a particular experiment. Any remaining biases must be corrected for in the bias term β. Low-altitude coastal sites or midcontinent sites far from pollution sources could also be used as background. It is, however, difficult to identify sites of these types which are not influenced by local sources. Conditional sampling only when meteorological conditions indicate air from a clean air sector could alleviate this problem. When CO_{2ff} at multiple surface locations is being

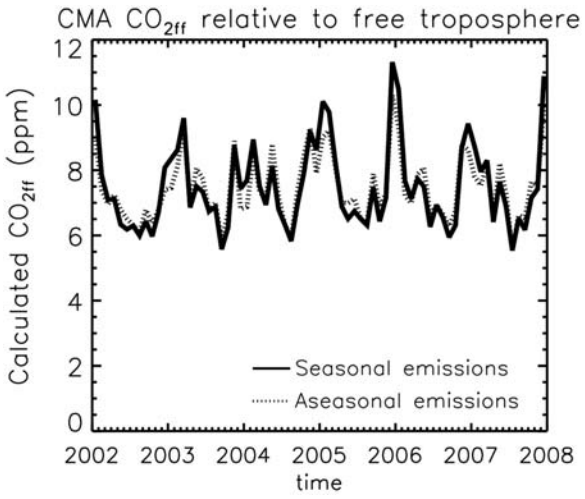

Figure 10. Calculated CO_{2ff} at CMA (using free troposphere above CMA as background) for our standard fluxes, including seasonally varying fossil fuel CO_2 flux, and when fossil fuel CO_2 emissions have no seasonality (aseasonal emissions).

compared, it may be most appropriate to select the "cleanest" of these sites as local background, rather than using a regional background site. In this case, any bias in the choice of background will be the same for all sites, allowing direct comparison between the various sites, but any seasonal or interannual bias in the chosen local background site would need to be carefully evaluated. Ultimately, methods of determining CO_{2ff} which are less reliant on the underlying Lagrangian assumption will be needed.

3.4. Effect of Other Fluxes (and Their Uncertainties) on Fossil Fuel CO_2 Calculation

[35] In our model, where the contributions of each ^{14}C source are quantified individually, we can determine the bias (β, second term in equation (1)) in the calculation of CO_{2ff} due to other sources of ^{14}C, which cannot be removed by judicious choice of background site. We calculate the effect of β on the determination of CO_{2ff} in boundary layer air, using free tropospheric air at 3.5 km above each site as the background, and the same example sites we discussed in section 3.3.

[36] We calculate CO_{2ff} when β is calculated from the model, and when β is neglected (Figure 9). The seasonal cycle in CO_{2ff} that arises is dominated by seasonal differences in atmospheric transport, and only weakly from the seasonality in the CO_{2ff} flux itself. For example, the modeled CO_{2ff} values at CMA are very similar when the CO_{2ff} flux is input into the model with no seasonality (Figure 10). When we separate the CO_{2ff} flux into CO_{2ff} fluxes from each continent (Europe-CO_{2ff}, North America-CO_{2ff}, etc, data not shown), we find that the majority of the seasonality in CO_{2ff} comes from the local continent, indicating that most of the seasonality at the surface comes from seasonal differences in venting of the boundary layer, with stronger venting in the summer reducing the surface CO_{2ff} mixing ratio. Only weak contributions to the surface seasonal cycle come from seasonally varying cross-tropopause exchange and free tropospheric transport.

[37] The effect of fossil fuel CO_2 dominates the calculation of CO_{2ff}, and β contributes only 10% of the signal in summer, and less than 2% in winter at these sites. The bias is driven by the gross biospheric ^{14}C flux, and we see no significant bias from the cosmogenic ^{14}C production flux, or from the oceans, even at Northern Hemisphere coastal sites. The model indicates a small bias from the nuclear industry, but even doubling of this flux would have only a minor effect. Our model evenly distributed the nuclear industry flux, and so does not capture the possibility of significant biases close to power plants, such as those observed and corrected for by *Levin et al.* [2003] and *Palstra et al.* [2008].

[38] In our standard scenario, at midlatitude Northern Hemisphere sites, the terrestrial biosphere contributes a positive bias of 0.5 ppm in summer, but less than 0.2 ppm in winter (Figure 9). This seasonal difference is due to the strong seasonality of biospheric respiration, which is largest in the summer months, and the magnitude of the bias is similar throughout the midlatitude Northern Hemisphere. Our sensitivity tests indicate that the highbio estimate of the biosphere flux would cause a consistent, positive summertime bias in CO_{2ff} of 0.8 ppm, with a much smaller bias of 0.3 ppm in winter (Figure 9, bottom). The lowbio scenario produces a bias of less than 0.4 ppm in summer and 0.2 ppm in winter. The apparent underestimate of vertical gradients in LMDZ will result in an underestimate of the fossil fuel CO_2 gradient and of the bias in our analysis; the magnitude of this problem is not well quantified, but is likely similar to, or smaller than the effect of the range of biosphere flux estimates we use. Thus a range of values for the bias is 0.4–0.8 ppm in summer, and 0.2–0.3 ppm in winter at these sites.

[39] This bias is quite consistent across most of the Northern Hemisphere land (Figure 11), except for higher

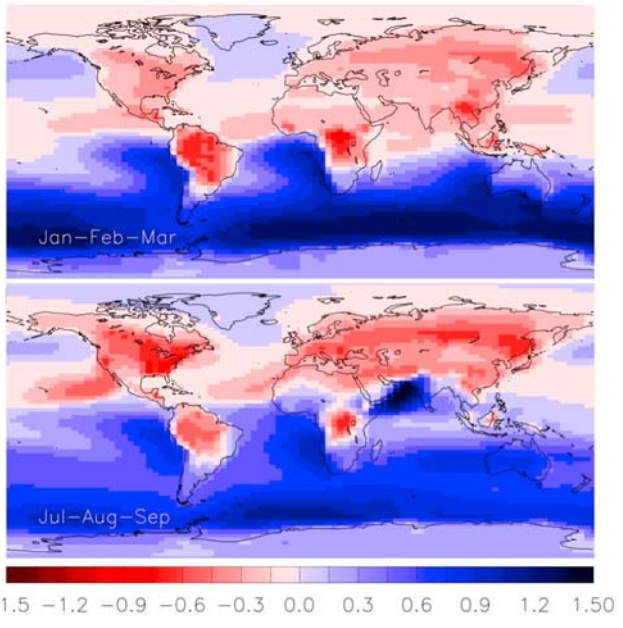

Figure 11. Northern Hemisphere (top) winter (January–February–March mean) and (bottom) summer (July–August–September mean) modeled bias in ppm of CO_{2ff} at the surface, when the 3.5 km free troposphere is used as background. The standard biosphere flux scenario is used.

values in the southeastern United States. Although we are able to estimate and correct for this bias using the model results, CO_{2ff} calculations will be less reliable when the bias term is large relative to CO_{2ff}. For example, $\Delta^{14}CO_2$ observations likely cannot be reliably used to determine fossil fuel CO_2 emissions in most of the Southern Hemisphere, where the ocean bias has similar magnitude to CO_{2ff}. Similarly, the tropics have lower CO_{2ff} emissions and high bias, due to the strong biospheric exchange there.

4. Conclusions

[40] Our model studies indicate that $\Delta^{14}CO_2$ does indeed provide a good tracer for recently added fossil fuel CO_2. CO_{2ff} accounts for almost all of the Northern Hemisphere $\Delta^{14}CO_2$ spatial variability, with only small contributions from other sources.

[41] When calculating the recently added fossil fuel CO_2 mixing ratio using $\Delta^{14}CO_2$, uncertainty is contributed by uncertainty in the $\Delta^{14}CO_2$ measurement, and from the choice of background site, and biases from other sources of ^{14}C.

[42] The choice of background site is critical to interpretation of the amount of "recently added" fossil fuel CO_2. Free tropospheric air appears to be a reasonable choice for background, if the biases, mainly from the terrestrial biosphere, are accounted for. Although high-altitude mountain sites currently provide the best estimates of clean background air, they may be influenced by local fossil fuel pollution, especially in summer. These differences are typically of the same magnitude as the current $\Delta^{14}CO_2$ measurement uncertainties, but may result in a bias rather than random noise. Therefore care must be taken in choosing the most appropriate background for each experiment. The uncertainty due to the choice of background site depends on the experimental design, when using mountain sites for background, but is likely less than 2‰ or 0.7ppm in CO_{2ff}.

[43] When the recently added fossil fuel CO_2 contribution is calculated using the commonly used pseudo-Lagrangian method described here, relative to remote (marine boundary layer, high altitude or free tropospheric) background sites, a small bias due mostly to terrestrial biospheric ^{14}C flux, is induced. In most temperate Northern Hemisphere regions, ignoring the bias would result in an underestimate of CO_{2ff} of 0.5 ppm in CO_{2ff} in summer, and 0.2 ppm in winter. Our model indicates that the maximum uncertainty in this bias is 0.3 ppm in summer and 0.1 ppm in winter. Some regions, notably the southeastern United States, have a higher bias in the summertime, and thus extra care must be taken in interpreting $\Delta^{14}CO_2$ observations in this region.

[44] When these biases are accounted for, the total uncertainty in the calculation of CO_{2ff} from $\Delta^{14}CO_2$ measurements of 2‰ precision is less than 1 ppm for a single observation, including uncertainty from the $\Delta^{14}CO_2$ measurement (0.7 ppm), uncertainty in the magnitude of the bias (0.3 ppm) and uncertainty in the choice of background site (0.7 ppm).

[45] Our results indicate that accurate estimates of the fossil fuel CO_2 mixing ratio, with quantified uncertainties, can be obtained from atmospheric samples. The challenge remains to infer fossil fuel CO_2 fluxes from this data. For small-scale studies, observationally obtained flux estimates from the radon method impart ~30% additional uncertainty in local flux estimates [*Levin et al.*, 1999] and plume measurements of city pollution combined with meteorological information obtain uncertainties in fluxes of ~50% [*Trainer et al.*, 1995]. For larger scales, atmospheric transport models are the most common approach. These models have significant errors with complex structure [*Stephens et al.*, 2007; *Gurney et al.*, 2002, 2004]. Interactions of seasonally varying biospheric fluxes and atmospheric transport contribute much of this uncertainty [*Gurney et al.*, 2002, Figure 3] and this will play a much smaller role for fossil fuel fluxes. Furthermore, recent comparisons of modeled CO_2 with observations [*Law et al.*, 2008; *Patra et al.*, 2008; *Lauvaux et al.*, 2008] suggest considerable improvement. Transport model error will likely still dominate any inversion study of fossil fuel fluxes from $\Delta^{14}CO_2$, but it seems unlikely to confound such an inversion. How much information the combined observation/modeling system will add to economically based inventories with their uncertainties of 5–20% [*Marland et al.*, 2006] must await properly formulated observing system simulation experiments.

[46] **Acknowledgments.** This paper was improved by thoughtful comments and suggestions by two anonymous reviewers. The Niwot Ridge time series includes some additional data not previously published. Thanks go to Scott Lehman, Chad Wolak, and the NOAA/ESRL Carbon Cycle team for providing these measurements. Some stratospheric $\Delta^{14}CO_2$ measurements were kindly provided by Takakiyo Nakazawa at Tohoku University.

References

Baker, D. F., et al. (2006), TransCom 3 inversion intercomparison: Impact of transport model errors on the interannual variability of regional CO_2 fluxes, 1988–2003, *Global Biogeochem. Cycles*, *20*, GB1002, doi:10.1029/2004GB002439.

Balshi, M. S., et al. (2007), The role of historical fire disturbance in the carbon dynamics of the pan-boreal region: A process-based analysis, *J. Geophys. Res.*, *112*, G02029, doi:10.1029/2006JG000380.

Blasing, T., C. Broniak, and G. Marland (2005), The annual cycle of fossil-fuel carbon dioxide emissions in the United States, *Tellus, Ser. B*, *57*, 107–115.

Bousquet, P., F. Delage, C. Carouge, L. Klenov, C. Aulagnier, M. Ramonet, and F. Chevallier (2008), Evaluation of the LMDZ model for the representation of the atmospheric CO_2 concentrations, report, 42 pp., Lab. des Sci. du Clim. et de l'Environn., Paris.

Braziunas, T. F., I. Y. Fung, and M. Stuiver (1995), The preindustrial atmospheric $^{14}CO_2$ latitudinal gradient as related to exchanges among atmospheric, oceanic and terrestrial reservoirs, *Global Biogeochem. Cycles*, *9*(4), 565–584, doi:10.1029/95GB01725.

Broecker, W. S., T.-H. Peng, H. Ostlund, and M. Stuiver (1985), The distribution of bomb radiocarbon in the ocean, *J. Geophys. Res.*, *90*(C4), 6953–6970, doi:10.1029/JC090iC04p06953.

Emanuel, K. A. (1991), A scheme for representing cumulus convection in large-scale models, *J. Atmos. Sci.*, *48*, 2313–2335, doi:10.1175/1520-0469(1991)048<2313:ASFRCC>2.0.CO;2.

Emanuel, K. A. (1993), A cumulus representation based on the episodic mixing model: The importance of mixing and microphysics in predicting humidity, *Meteorol. Monogr.*, *24*(46), 185–192.

Gaudinski, J. B., S. E. Trumbore, E. A. Davidson, and S. Zheng (2000), Soil carbon cycling in a temperate forest: Radiocarbon-based estimates of residence times, sequestration rates and partitioning of fluxes, *Biogeochemistry*, *51*, 33–69, doi:10.1023/A:1006301010014.

Geels, C., et al. (2007), Comparing atmospheric transport models for future regional inversions over Europe—Part 1: Mapping the atmospheric CO_2 signals, *Atmos. Chem. Phys.*, *7*, 3461–3479.

Godwin, H. (1962), Half-life of radiocarbon, *Nature*, *195*, 984, doi:10.1038/195984a0.

Graven, H. D., T. P. Guilderson, and R. F. Keeling (2007), Methods for high-precision ^{14}C AMS measurement of atmospheric CO_2 at LLNL, *Radiocarbon*, *49*(2), 349–356.

Gregg, J. S., R. J. Andres, and G. Marland (2008), China: Emissions pattern of the world leader in CO2 emissions from fossil fuel consumption and cement production, *Geophys. Res. Lett.*, *35*, L08806, doi:10.1029/2007GL032887.

Gurney, K. R., et al. (2002), Towards robust regional estimates of CO_2 sources and sinks using atmospheric transport models, *Nature*, *415*, 626–630, doi:10.1038/415626a.

Gurney, K. R., et al. (2004), Transcom 3 inversion intercomparison: Model mean results for the estimation of seasonal carbon sources and sinks, *Global Biogeochem. Cycles*, *18*, GB1010, doi:10.1029/2003GB002111.

Hahn, V., and N. Buchmann (2004), A new model for soil organic carbon turnover using bomb carbon, *Global Biogeochem. Cycles*, *18*, GB1019, doi:10.1029/2003GB002115.

Hauglustaine, D., F. Hourdin, L. Jourdain, M.-A. Filiberti, S. Walters, J.-F. Lamarque, and E. Holland (2004), Interactive chemistry in the Laboratoire de Meteorologie Dynamique general circulation model: Description and background tropospheric chemistry evaluation, *J. Geophys. Res.*, *109*, D04314, doi:10.1029/2003JD003957.

Hesshaimer, V., M. Heimann, and I. Levin (1994), Radiocarbon evidence for a smaller oceanic carbon dioxide sink than previously believed, *Nature*, *370*, 201–203, doi:10.1038/370201a0.

Hourdin, F., et al. (2006), The LMDZ4 general circulation model: Climate performance and sensitivity to parameterized physics with emphasis on tropical convection, *Clim. Dyn.*, *27*(7–8), 787–813, doi:10.1007/s00382-006-0158-0.

Hsueh, D. Y., N. Y. Krakauer, J. T. Randerson, X. Xu, S. E. Trumbore, and J. R. Southon (2007), Regional patterns of radiocarbon and fossil fuel-derived CO_2 in surface air across North America, *Geophys. Res. Lett.*, *34*, L02816, doi:10.1029/2006GL027032.

International Atomic Energy Agency (IAEA) (2004), *Management of waste containing tritium and carbon-14*, *Tech. Rep. Ser. 421*, 109 pp., Vienna.

Karlen, I., I. U. Olsson, P. Kllburg, and S. Kilici (1968), Absolute determination of the activity of two ^{14}C dating standards, *Ark. Geofys.*, *4*, 465–471.

Krakauer, N., J. T. Randerson, F. W. Primeau, N. Gruber, and D. Menemenlis (2006), Carbon isotope evidence for the latitudinal distribution of wind speed dependence of the air-sea gas transfer velocity, *Tellus, Ser. B*, *58*, 390–417, doi:10.1111/j.1600-0889.2006.00223.x.

Kuc, T., K. Rozanski, M. Zimnoch, J. Necki, L. Chmura, and D. Jelen (2007), Two decades of regular observations of $^{14}CO_2$ and $^{13}CO_2$ content in atmospheric carbon dioxide in central Europe: Long-term changes of regional anthropogenic fossil CO_2 emissions, *Radiocarbon*, *49*(2), 807–816.

Lal, D. (1988), Theoretically expected variations in the terrestrial cosmic-ray production rates of isotopes, in *Proceedings of the International School of Physics, Solar-Terrestrial Relationships and the Earth Environment in the Last Millennia*, edited by G. Cini Castagnoli, pp. 215–233, Elsevier, Amsterdam.

Lauvaux, T., M. Uliasz, C. Sarrat, F. Chevallier, P. Bousquet, C. Lac, K. J. Davis, P. Ciais, A. S. Denning, and P. J. Rayner (2008), Mesoscale inversion: First results from the CERES campaign with synthetic data, *Atmos. Chem. Phys.*, *8*, 3459–3471.

Law, R. M., et al. (2008), TransCom model simulations of hourly atmospheric CO_2: Experimental overview and diurnal cycle results for 2002, *Global Biogeochem. Cycles*, *22*, GB3009, doi:10.1029/2007GB003050.

Levin, I., and U. Karstens (2007), Inferring high-resolution fossil fuel CO_2 records at continental sites from combined $^{14}CO_2$ and CO observations, *Tellus, Ser. B*, *59*, 245–250.

Levin, I., and B. Kromer (1997), Twenty years of atmospheric $^{14}CO_2$ observations at Schauinsland station, Germany, *Radiocarbon*, *39*(2), 205–218.

Levin, I., and B. Kromer (2004), The tropospheric $^{14}CO_2$ level in mid-latitudes of the Northern Hemisphere (1959–2003), *Radiocarbon*, *46*(3), 1261–1272.

Levin, I., and C. Rödenbeck (2007), Can the envisaged reductions in fossil fuel CO_2 emissions be detected using atmospheric observations?, *Naturwissenschaften*, *95*(3), 203–208, doi:10.1007/s00114-007-0313-4.

Levin, I., B. Kromer, H. Schoch-Fischer, M. Bruns, M. Munnich, D. Berdau, J. C. Vogel, and K. O. Munnich (1985), 25 years of tropospheric ^{14}C observations in central Europe, *Radiocarbon*, *27*(1), 1–19.

Levin, I., H. Glatzel-Mattheier, T. Marik, M. Cuntz, M. Schmidt, and D. E. Worthy (1999), Verification of German methane emission inventories and their recent changes based on atmospheric observations, *J. Geophys. Res.*, *104*(D3), 3447–3456, doi:10.1029/1998JD100064.

Levin, I., B. Kromer, M. Schmidt, and H. Sartorius (2003), A novel approach for independent budgeting of fossil fuel CO_2 over Europe by $^{14}CO_2$ observations, *Geophys. Res. Lett.*, *30*(23), 2194, doi:10.1029/2003GL018477.

Levin, I., S. Hammer, B. Kromer, and F. Meinhardt (2008), Radiocarbon observations in atmospheric CO_2: Determining fossil fuel CO_2 over Europe using Jungfraujoch observations as background, *Sci. Total Environ.*, *391*(2–3), 211–216, doi:10.1016/j.scitotenv.2007.10.019.

Lugauer, M., U. Baltensperger, M. Furger, H. Gäggeler, D. Jost, M. Schwikowski, and H. Wanner (1998), Aerosol transport to the high Alpine sites Jungfraujoch (3454 m asl) and Colle Gnifetti (4452 m asl), *Tellus, Ser. B*, *50*, 76–92.

Lugauer, M., U. Baltensperger, M. Furger, H. Gäggeler, D. Jost, S. Nyeki, and M. Schwikowski (2000), Influences of vertical transport and scavenging on aerosol particle surface area and radon decay product concentrations at the Jungfraujoch (3452 m above sea level), *J. Geophys. Res.*, *105*(D15), 19,869–19,879, doi:10.1029/2000JD900184.

Manning, M. R., D. C. Lowe, W. H. Melhuish, R. J. Sparks, G. Wallace, C. A. M. Brenninkmeijer, and R. C. McGill (1990), The use of radiocarbon measurements in atmospheric sciences, *Radiocarbon*, *32*(1), 37–58.

Marland, G., T. A. Boden, and R. J. Andres (2006), Global, regional and national CO_2 emissions, in *Trends: A Compendium of Data on Global Change*, edited by T. A. Boden et al., pp. 505–584, Carbon Dioxide Inf. Anal. Cent., Oak Ridge Natl. Lab., U.S. Dep. of Energy, Oak Ridge, Tenn.

Masarik, J., and J. Beer (1999), Simulation of particle fluxes and cosmogenic nuclide formation in the Earth's atmosphere, *J. Geophys. Res.*, *104*(D10), 12,099–12,111, doi:10.1029/1998JD200091.

Meijer, H. A. J., H. M. Smid, E. Perez, and M. G. Keizer (1996), Isotopic characterization of anthropogenic CO_2 emissions using isotopic and radiocarbon analysis, *Phys. Chem. Earth*, *21*(5–6), 483–487, doi:10.1016/S0079-1946(97)81146-9.

Müller, S., F. Joos, G.-K. Plattner, N. Edwards, and T. F. Stocker (2008), Modeled natural and excess radiocarbon: Sensitivities to the gas exchange formulation and ocean transport strength, *Global Biogeochem. Cycles*, *22*, GB3011, doi:10.1029/2007GB003065.

Naegler, T., and I. Levin (2006), Closing the global radiocarbon budget 1945–2005, *J. Geophys. Res.*, *111*, D12311, doi:10.1029/2005JD006758.

Naegler, T., and I. Levin (2009), Biosphere-atmosphere gross carbon exchange flux and the $\delta^{13}CO_2$ and $\Delta^{14}CO_2$ disequilibria constrained by the biospheric excess radiocarbon inventory, *J. Geophys. Res.*, *114*, D17303, doi:10.1029/2008JD011116.

Naegler, T., P. Ciais, K. Rodgers, and I. Levin (2006), Excess radiocarbon constraints on air-sea gas exchange and the uptake of CO_2 by the oceans, *Geophys. Res. Lett.*, *33*, L11802, doi:10.1029/2005GL025408.

Nakamura, T., T. Nakazawa, N. Nakai, H. Kitigawa, H. Honda, T. Itoh, T. Machida, and E. Matsumoto (1992), Measurement of ^{14}C concentrations of stratospheric CO_2 by accelerator mass spectrometry, *Radiocarbon*, *34*(3), 745–752.

Nakamura, T., T. Nakazawa, H. Honda, H. Kitagawa, T. Machida, A. Ikeda, and E. Matsumoto (1994), Seasonal variations in ^{14}C concentrations of stratospheric CO_2 measured with accelerator mass spectrometry, *Nucl. Instrum. Methods Phys. Res., Sect. B*, *92*, 413–416.

Nydal, R., and K. Lövseth (1983), Tracing bomb ^{14}C in the atmosphere 1962–1980, *J. Geophys. Res.*, *88*(C6), 3621–3642, doi:10.1029/JC088iC06p03621.

Olivier, J. G. J., and J. J. M. Berdowski (2001), Global emissions sources and sinks, in *The Climate System*, edited by J. Berdowski et al., pp. 33–78, A. A. Balkema, Lisse, Netherlands.

Palstra, S. W., U. Karstens, H.-J. Streurman, and H. A. J. Meijer (2008), Wine ethanol ^{14}C as a tracer for fossil fuel CO_2 emissions in Europe: Measurements and model comparison, *J. Geophys. Res.*, *113*, D21305, doi:10.1029/2008JD010282.

Patra, P. K., et al. (2008), TransCom model simulations of hourly atmospheric CO_2: Analysis of synoptic-scale variations for the period 2002–2003, *Global Biogeochem. Cycles*, *22*, GB4013, doi:10.1029/2007GB003081.

Peylin, P., et al. (2009), Importance of fossil fuel emissions uncertainties over Europe for CO_2 modeling: Model intercomparison, *Atmos. Chem. Phys. Discuss.*, *9*, 7457–7503.

Randerson, J., I. G. Enting, E. A. G. Schuur, K. Caldeira, and I. Y. Fung (2002), Seasonal and latitudinal variability of troposphere $\Delta^{14}CO_2$: Post bomb contributions from fossil fuels, oceans, the stratosphere, and the terrestrial biosphere, *Global Biogeochem. Cycles*, *16*(4), 1112, doi:10.1029/2002GB001876.

Riley, W. G., D. Y. Hsueh, J. T. Randerson, M. L. Fischer, J. Hatch, D. E. Pataki, W. Wang, and M. L. Goulden (2008), Where do fossil fuel carbon dioxide emissions from California go? An analysis based on radiocarbon observations and an atmospheric transport model, *J. Geophys. Res.*, *113*, G04002, doi:10.1029/2007JG000625.

Stephens, B. B., et al. (2007), Weak northern and strong tropical land carbon uptake from vertical profiles of atmospheric CO_2, *Science*, *316*, 1732–1735, doi:10.1126/science.1137004.

Stohl, A. (2001), A 1-year Lagrangian "climatology" of airstreams in the Northern Hemisphere troposphere and lowermost stratosphere, *J. Geophys. Res.*, *106*(D7), 7263–7279, doi:10.1029/2000JD900570.

Stuiver, M., and H. A. Polach (1977), Discussion: Reporting of ^{14}C data, *Radiocarbon*, *19*(3), 355–363.

Stuiver, M., P. Quay, and H. Ostlund (1983), Abyssal water carbon-14 distribution and the age of the world oceans, *Science*, *219*, 849–851, doi:10.1126/science.219.4586.849.

Suess, H. E. (1955), Radiocarbon concentration in modern wood, *Science*, *122*, 415–417, doi:10.1126/science.122.3166.415-a.

Sweeney, C., M. Gloor, A. R. Jacobson, R. M. Key, G. McKinley, J. L. Sarmiento, and R. Wanninkhof (2007), Constraining global air-sea gas exchange for CO_2 with recent bomb ^{14}C measurements, *Global Biogeochem. Cycles*, *21*, GB2015, doi:10.1029/2006GB002784.

Takahashi, H. A., E. Konohira, T. Hiyama, M. Minami, T. Nakamura, and N. Yoshida (2002), Diurnal variation of CO_2 concentration, $\Delta^{14}C$ and $\delta^{13}C$ in an urban forest: Estimate of the anthropogenic and biogenic CO_2 contributions, *Tellus, Ser. B*, *54*, 97–109.

Taylor, K. E. (2001), Summarizing multiple aspects of model performance in a single diagram, *J. Geophys. Res.*, *106*(D7), 7183–7192, doi:10.1029/2000JD900719.

Thompson, M. V., and J. T. Randerson (1999), Impulse response functions of terrestrial carbon cycle models: Method and application, *Global Change Biol.*, *5*, 371–394, doi:10.1046/j.1365-2486.1999.00235.x.

Trainer, M., B. Ridley, M. Buhr, G. Kok, J. Walega, G. Hübler, D. D. Parrish, and F. Fehsenfeld (1995), Regional ozone and urban plumes in the southeastern United States: Birmingham, a case study, *J. Geophys. Res.*, *100*(D9), 18,823–18,834, doi:10.1029/95JD01641.

Trumbore, S. E. (2000), Age of soil organic matter and soil respiration: Radiocarbon constraints on belowground C dynamics, *Ecol. Appl.*, *10*(2), 399–411, doi:10.1890/1051-0761(2000)010[0399:AOSOMA]2.0.CO;2.

Turnbull, J. C. (2006), Development of a high precision $^{14}CO_2$ measurement capability and application to carbon cycle studies, Ph.D. thesis, 132 pp., Univ. of Colo., Boulder.

Turnbull, J. C., J. B. Miller, S. J. Lehman, P. P. Tans, R. J. Sparks, and J. R. Southon (2006), Comparison of $^{14}CO_2$, CO and SF_6 as tracers for determination of recently added fossil fuel CO_2 in the atmosphere and implications for biological CO_2 exchange, *Geophys. Res. Lett.*, *33*, L01817, doi:10.1029/2005GL024213.

Turnbull, J. C., S. J. Lehman, J. B. Miller, R. J. Sparks, J. R. Southon, and P. P. Tans (2007), A new high precision $^{14}CO_2$ time series for North American continental air, *J. Geophys. Res.*, *112*, D11310, doi:10.1029/2006JD008184.

Turnbull, J. C., et al. (2009), Spatial distribution of $\Delta^{14}CO_2$ across Eurasia: Measurements from the TROICA-8 expedition, *Atmos. Chem. Phys.*, *9*, 175–187.

UNSCEAR (2000), UNSCEAR 2000 report to the General Assembly, vol. II, Annex C, U.N. Sci. Comm. on the Effects of At. Radiat., Vienna.

Wanninkhof, R. (1992), Relationship between wind-speed and gas-exchange over the ocean, *J. Geophys. Res.*, *97*(C5), 7373–7382, doi:10.1029/92JC00188.

Zondervan, A., and H. A. J. Meijer (1996), Isotopic characterization of CO_2 sources during regional pollution events using isotopic and radiocarbon analysis, *Tellus, Ser. B*, *48*, 601–612.

P. Ciais, A. Cozic, and P. Rayner, Laboratoire des Sciences du Climat et de l'Environnement, F-91191 Gif-sur-Yvette, France.

J. Miller and J. Turnbull, Earth Systems Research Laboratory, NOAA, 325 Broadway, Boulder, CO 80303, USA. (jocelyn.turnbull@noaa.gov)

T. Naegler, Institut für Umweltphysik, INF 229, D-69120 Heidelberg, Germany.